REVIEW ARTICLE

Ideal collimation, concentration, and imaging with curved diffractive optical elements

Nándor Bokor[a)]
Department of Physics, Budapest University of Technology and Economics, Budafoki u. 8., 1111 Budapest, Hungary

Nir Davidson
Department of Physics of Complex Systems, Weizmann Institute of Science, 76100 Rehovot, Israel

(Received 24 May 2005; accepted 1 October 2005; published online 17 November 2005)

In this article the design, optimization and characterization of diffractive optical elements formed on a curved surface are reviewed. For such curved diffractive optical elements not only the phase function, but also the surface shape are free parameters that can be used for optimization, yielding much better performances than both flat diffractive optical elements and reflective/refractive optical elements when operating with quasimonochromatic light. We present a new analytic design approach for the surface shape that ensures uniform collimation of a light source with any angular distribution. We demonstrate the usefulness of this design also for ideal (brightness conserving) collimation and concentration of diffuse light, aberration-free imaging, and optical Fourier transform. We present experimental results that confirm our theoretical analysis. © *2005 American Institute of Physics.* [DOI: 10.1063/1.2127908]

I. INTRODUCTION

For conventional optical elements that rely on reflective or refractive surfaces, the optical performance is strictly dictated by the shape of those surfaces. For example, a reflective surface that focuses a collimated beam into an ideal (diffraction limited) spot must be a parabola. Such a parabolic mirror (PM), although commonly used, has several severe drawbacks that limit its usefulness. For imaging applications it suffers from large first-order aberrations for off-axis beams. When used for concentration of diffuse light (e.g., solar light) on a small target, it yields spot sizes substantially larger than those limited by the second law of thermodynamics (as explained in detail in Sec. II). Finally, for the "reverse" operation of collimating the light emitted from a small source, it yields a collimated beam with nonuniform intensity profile even for a source with uniform (angular) emission.

Alternatively, for diffractive optical elements (DOEs) that rely on diffractive surfaces, the optical performance is determined by both the shape of the surface and the phase function recorded on it. Hence, unlike for conventional optical elements, for a DOE fabricated on a curved surface—i.e. for curved diffractive optical elements (CDOEs)—the shape of the surface provides an additional, and often independent degree of freedom. It can thus be used for optimization, yielding much better performances than either flat DOEs or reflective/refractive optical elements, when operating with quasimonochromatic light. For example, recording the interference pattern of a spherical wave emitted from a point source and a perfectly collimated plane wave on a thin surface yields a CDOE that perfectly focuses that plane wave into an ideal (diffraction limited) spot regardless of the shape of the surface. The shape of the surface can then be independently optimized, e.g., to suppress first order off-axis aberrations in imaging applications, and for ideal concentration and uniform collimation of diffuse (but still quasimonochromatic) light.

The importance of the surface shape of such a thin CDOE is further illustrated by noting that it corresponds closely to the principal surface[1] or equivalent refracting locus[2] of an imaging system. The shape of the principal surfaces are known to have a profound effect on the aberration characteristics of the imaging system eliminating, e.g., first-order transverse aberrations if the principal surface satisfies the Abbe sine condition[1] and eliminating first-order axial aberrations if the principal surface satisfies the Herschel condition.[3,4]

In this review article we illustrate the flexibility and usefulness of CDOEs for ideal concentration and collimation of diffuse light at the theoretical limit imposed by the second law of thermodynamics, for aberration-free imaging, and for optical Fourier transform, areas for which CDOEs appear to be ideally suited.

First, in Sec. II we give a theoretical background for diffuse light concentration, discussing the relevant concepts of phase-space volume, phase-space area, brightness, and the thermodynamic limit on diffuse light concentration. A more comprehensive review on diffuse light concentration can be found in Ref. 5.

In Sec. III we present and illustrate a new design principle that was recently developed[6] for CDOEs that uniformly

[a)]Author to whom correspondence should be addressed; electronic mail: n_bokor@yahoo.com

collimates light emitted by arbitrarily shaped elongated Lambertian sources in one transverse direction [so called one-dimensional (1D) collimation]. By simply reversing the direction of the light rays we then show that CDOEs obtained from this design principle are also capable of ideal 1D concentration of diffuse light on arbitrarily shaped Lambertian targets.

In Sec. IV we describe a generalization of the CDOE design principle of Sec. III for finite distance concentration, and illustrate the usefulness of the principle for efficient and uniform side pumping of solid state lasers, so as to overcome some of the main limitations of existing laser pump cavities based on conventional elliptical mirrors.

In Sec. V we discuss a special case of the uniform collimator/concentrator CDOE design of the preceding sections, in which both the target and the source are flat surfaces. We show that in this case the CDOE shape satisfies the Abbe sine condition, so that the design principles presented in Secs. III and IV can be considered generalizations of the Abbe sine condition. We review experimental and theoretical studies that have been performed for such Abbe-type CDOEs, for diffuse light concentration, aberration-free imaging, and optical Fourier transform.

In Sec. VI we discuss the possibilities to extend the CDOE design principles of Secs. III and IV for 2D concentration, with special emphasis on the effect of skew rays. In Sec. VII we conclude, and in the Appendix we present some mathematical proofs concerning the design principles of Secs. III, IV, and VI.

CDOEs have several additional applications which are not discussed in this article, but are covered in detail in a review article elsewhere.[7] For example, the curved gratings invented by Rowland[8] are widely used in spectroscopy, especially in the far-ultraviolet regime.[9,10] CDOEs fabricated on existing curved substrates (windshields, swimming goggles, etc.) have been considered for visual display applications.[11] CDOEs can be used to control the geometrical apodization factor in high numerical aperture focusing systems,[3,12] and they can be applied for optical transformations.[13]

We do not put emphasis on fabrication methods. We briefly mention that holography is a simple and flexible tool to record the phase function on the CDOE, provided that a substrate of the given shape can be coated with the recording material. For surfaces with zero curvature, such as a cylinder, this can be done, e.g., by gluing a photopolymer film to the substrate,[14] whereas for surfaces with nonzero curvature, like a sphere, dip-coating processes can be used. For many applications readily available spherical/cylindrical and plane waves can be used to record the phase function holographically, without the need for complicated aspherical elements. Moreover, the performance of the CDOE often depends only weakly on the exact shape of the substrate, and hence the fabricated shape does not have to be accurate within optical precision, as long as it is identical during recording and readout. Lithographic processes can also be used for fabricating CDOEs having axial symmetry.[15]

Throughout the article we resort only to geometrical optics, since for the diffuse light applications we discuss the geometrical diffuse angles are much larger than the diffraction limited ones. Moreover, we limit the discussion to quasi-monochromatic light to suppress the large chromatic aberration of DOEs. We also assume that the thickness of the CDOE is small compared to its lateral size, and hence the deflection angle of the diffracted rays only depends on the lateral properties (period and orientation) of the local grating, whereas the depth properties (e.g., the surface relief profile, or the number and refractive index of Bragg surfaces) determines the local diffraction efficiency. In all the discussions we assume 100% diffraction efficiency, but the effect of non-ideal diffraction efficiencies can be readily incorporated in the analysis.

II. BASIC CONCEPTS AND LIMITATIONS FOR DIFFUSE LIGHT CONCENTRATION

The term diffuse light refers to light beams for which the geometrical diffusive angles and spot sizes are much larger than the diffraction limited ones. This means that the transverse (spatial) coherence length of the beam is much smaller than its size, and geometrical optics approximation and ray-tracing techniques can be used to describe the beam propagation. Whereas some diffuse light sources, such as the sun and thermal light bulbs emit polychromatic light and hence require refractive or reflective optical elements, other diffuse sources emit (quasi-)monochromatic light and can hence be manipulated also with diffractive optical elements that otherwise have large chromatic aberrations. Examples for such (quasi-)monochromatic diffuse light sources are high power diode laser bars, light emitting diodes (LEDs), and optically filtered sources.

Following Winston and Welford,[16] we define the four-dimensional phase-space volume (PSV) (also referred to as "étendue") of a diffuse beam as

$$\mathrm{PSV} = \int_x \int_y \int_{\sin \epsilon_x} \int_{\sin \epsilon_y} n^2 \cdot dx' \cdot dy' \cdot d(\sin \epsilon_x') \cdot d(\sin \epsilon_y'), \tag{1}$$

where x and y are the sizes, and ϵ_x and ϵ_y the half-divergence angles, of the beam in two orthogonal directions (both perpendicular to the direction of beam propagation), and n is the index of refraction. In general a diffuse beam is characterized by a nonuniform distribution function $I(x,y,\epsilon_x,\epsilon_y)$. Space-invariant diffusivity means that the distribution function can be written as a product of two distributions: $I_1(x,y)\cdot I_2(\epsilon_x,\epsilon_y)$. For a beam with uniform and space-invariant diffusivity PSV is the product of the phase-space areas (PSAs) in the x and y directions, defined as

$$\mathrm{PSA}_x = \sqrt{\pi}\cdot n \cdot x \cdot \sin \epsilon_x, \quad \mathrm{PSA}_y = \sqrt{\pi}\cdot n \cdot y \cdot \sin \epsilon_y. \tag{2}$$

The optical brightness B (also referred to as radiance) is then defined as the power per unit area per unit solid angle

$$B = \frac{P}{\mathrm{PSV}}, \tag{3}$$

where P is the optical power transmitted by the beam. A fundamental conservation law, closely related to the second law of thermodynamics, states that for spatially incoherent

light and passive linear optical transformations the brightness cannot increase. In the optimal case brightness is conserved. Conservation of brightness is analogous to Liouville's theorem for Hamiltonian systems in statistical mechanics. Liouville's theorem formulates conservation of density of $6N$-dimensional phase space, where N is the number of particles in the system.

For lossless transformations P is constant and conservation of brightness implies a conservation of PSV. This so-called étendue invariance[16] imposes a fundamental theoretical limit—called the thermodynamic limit—on the maximum concentration ratio $\mathrm{CR}_{\max}$ that can be achieved for diffuse light concentration:

$$\mathrm{CR}_{\max} = \left(\frac{x_{\mathrm{in}} y_{\mathrm{in}}}{x_{\mathrm{out}} y_{\mathrm{out}}}\right)_{\max} = \frac{n_{\mathrm{out}}^2}{n_{\mathrm{in}}^2} \cdot \frac{1}{\sin \epsilon_x \sin \epsilon_y}. \tag{4}$$

ϵ_x and ϵ_y are the half divergence angles of the incoming beam. Throughout the present article we only deal with systems in which $n_{\mathrm{in}} = n_{\mathrm{out}}$ (i.e., the source and the target are in the same medium), but we briefly note here that—as seen in Eq. (4)—in the general case a factor of $n_{\mathrm{out}}^2/n_{\mathrm{in}}^2$ can be gained in $\mathrm{CR}_{\max}$ by placing the source and the target in media having different indices of refraction.

If the beam is concentrated only in one of the transverse directions, say in x, then the 1D thermodynamic limit for concentration ratio is

$$\mathrm{CR}_{\max} = \left(\frac{x_{\mathrm{in}}}{x_{\mathrm{out}}}\right)_{\max} = \frac{1}{\sin \epsilon_x}. \tag{5}$$

For both the 1D and the 2D cases we define the normalized concentration ratio as $\mathrm{CR}/\mathrm{CR}_{\max}$, so that it is equal to unity at the thermodynamic limit.

Since PSA_x and PSA_y need not be individually conserved (only their product, PSV, must be conserved) 1D concentration can actually overcome the thermodynamic limit of Eq. (5), whereby PSA_x can be reduced at the expense of increasing PSA_y, for example, by anamorphic beam shaping devices.[17] Note that in the common terminology of the literature[5] "1D concentration," i.e., concentration along one spatial direction, is achieved by "2D concentrator shapes" $z(x)$, whereas "2D concentration" is achieved by "3D concentrator shapes" $z(x,y)$.

Although in many applications light is concentrated on flat targets (e.g., detectors, solar cells), for other applications, such as cylindrical water pipes and cylindrical laser rods, 1D concentration is done on a curved target. In such cases the thermodynamic limit on concentration Eq. (5) must be applied to the circumference length of the target.

Conventional imaging optical elements such as imaging lenses and parabolic mirrors are commonly used for concentration of diffused light both in one and two dimensions. However, their maximum concentration ratio falls substantially below the thermodynamic limit, for reasons that can be related to aberrations of the imaging condition for light rays with off-axis angles. Nonimaging concentrators perform much better and in some cases approach the thermodynamic limit.[5] However, for incoming diffuse beams with small diffusive angles, their overall length becomes extremely large, and often requires additional stages of preconcentration so as to achieve an overall system with reasonably compact dimensions. It is exactly this limit of small diffuse angles where CDOEs perform best, while maintaining very compact dimensions, as shown in Secs. III–V.

An important and powerful tool for the design of diffuse light concentrators is the edge-ray principle:[5] if the concentrator directs the extreme incident rays (at angles $\pm\epsilon_x$) exactly tangent to the target then all intermediate rays—and hence all of the incident energy—hit the target too. This principle was successfully applied to the design of reflective concentrators such as the compound parabolic concentrator[5] and it is very useful for CDOEs too, as shown in Sec. III. While for 1D concentration the edge-ray principle strictly holds, it is not always applicable for 2D concentration (and 3D concentrator shapes), even when they have cylindrical symmetry. The reason for this is the effect of skew rays (rays that are not in the same plane as the symmetry axis of the system). Such rays were shown to impair the performance of reflective concentrators,[16] and their effect on 3D CDOEs is discussed in Sec. VI.

With the opposite process of transforming diffuse light emitted by a finite size source into a nearly collimated light beam, the goal is to obtain a collimated output beam with a minimum angular spread. By using the properties of diffuse light concentration presented above and simply reversing the direction of the light beams, it can be seen that for a given source circumference x_{in} and collimated output beam size x_{out} the minimum achievable diffusive angle of the collimated output beam is

$$\epsilon_{\min} = \sin^{-1}\left(\frac{x_{\mathrm{in}}}{x_{\mathrm{out}}}\right). \tag{6}$$

Equation (6) is the thermodynamic limit for diffuse light collimation, and is equivalent to Eq. (5), the thermodynamic limit for diffuse light concentration.

For finite distance concentration—discussed in Sec. IV—the thermodynamic limit for Lambertian sources and targets is

$$\mathrm{CR}_{\max} = \left(\frac{x_{\mathrm{in}}}{x_{\mathrm{out}}}\right)_{\max} = 1, \tag{7}$$

so that light cannot be concentrated onto a target having a smaller circumference than that of the source (without a loss in power). An example for finite distance concentrators is a reflecting tube with elliptical cross section, widely used for the side pumping of solid state lasers. This elliptical cavity, however, works ideally only for point-like sources and targets. Different magnifications of different portions of the ellipse make the performance of the elliptical cavity significantly worse than the thermodynamic limit Eq. (7). An additional drawback of such concentrators is the highly nonuniform intensity profile on the target. On the other hand, concentration reaching the thermodynamic limit [Eq. (7)] and with a uniform pump density profile can be achieved with CDOEs, as shown in Sec. IV.

Finally, we note that conservation of brightness applies both globally and locally. Thus, if the input beam is uniform in phase space then only a concentrator/collimator that retains the uniformity of phase space can achieve conservation

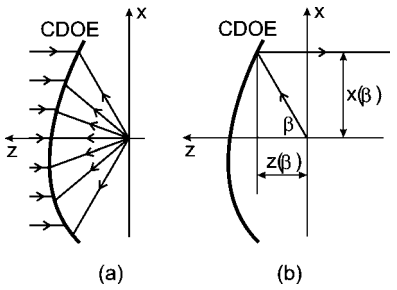

FIG. 1. (a) Recording and (b) readout geometry of a holographic CDOE of shape $z(x)$, working as a collimator. β is the angle between the direction of a reconstructing ray and the z axis. The corresponding coordinates of the CDOE surface are $x(\beta)$ and $z(\beta)$.

of brightness. In such cases uniform concentrators/collimators are necessary (although not always sufficient) to achieve ideal concentration/collimation at the thermodynamic limit, as proved analytically in the Appendix.

III. UNIFORM COLLIMATION AND IDEAL COLLIMATION AND CONCENTRATION IN ONE DIMENSION WITH CDOEs

Plane wave illumination with uniform intensity is of great importance in many areas of optics. A point source can be simply collimated with a PM that reflects all rays originating from the focal point into the same direction without any aberrations. However, even for isotropic point sources, the PM yields a collimated beam of nonuniform intensity. The essence of the problem here is that the shape of the mirror required for collimation is uniquely determined by Snell's reflection law to be a parabola, whereas uniform intensity of the reflected light requires a different reflector shape.[6]

In this section we present the design principle of a CDOE that can independently fulfill the two requirements for quasimonochromatic light: its shape ensures uniform illumination for arbitrarily shaped diffuse sources, and its phase function ensures optimal collimation.[6] Extension of the method for any specific nonuniform illumination is straightforward. We then show that such a CDOE, when operated in reverse, can serve as an ideal concentrator that efficiently concentrates diffuse light at the thermodynamic limit defined in Sec. II.

The geometric arrangements for recording and readout of a curved reflective holographic collimator operating in one dimension are shown in Fig. 1. Figure 1(a) shows a recording arrangement of the interference of a plane wave and a counterpropagating cylindrical wave on a holographic film with shape $z(x)$. Figure 1(b) shows the readout arrangement with the same diverging cylindrical wave. As seen, the first diffraction order yields a perfectly collimated plane wave, regardless of the CDOE's shape. Note that this readout geometry also automatically fulfills the Bragg condition for the entire CDOE, hence permitting high diffraction efficiencies. The shape $z(x)$ can now be designed to yield uniform intensity of the collimated beam for a given illumination source. This is in contrast to a reflective mirror whose shape must be a parabola to ensure exact collimation.

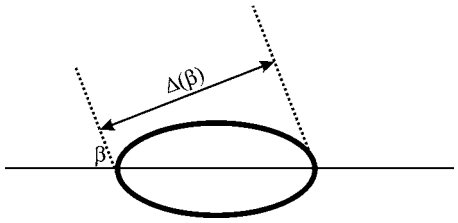

FIG. 2. Schematic diagram of an elongated Lambertian source whose angular intensity distribution is proportional to $\Delta(\beta)$, the projected diameter of the cross section of the source as seen from direction β.

In order to determine the shape $z(x)$ we consider a small source located at $x=0$, $z=0$, and emitting radiation in the (x,z) plane with angular (far-field) intensity distribution $S(\beta)$, where β is the angle between the direction of the radiation and the z axis, as shown in Fig. 1. For an isotropic point source $S(\beta)=$constant, for a planar diffuse Lambertian source $S(\beta)\propto\cos\beta$, and for general elongated Lambertian sources, shown in Fig. 2, $S(\beta)\propto\Delta(\beta)$, where $\Delta(\beta)$ is the projected diameter of the source as seen from direction β. For a cylindrical Lambertian source $S(\beta)=$constant, the same as for an isotropic point source. If $I(x)$ is the local intensity of the output beam at vertical coordinate x, then from energy conservation we get

$$S(\beta)d\beta = I(x)dx. \tag{8}$$

To ensure uniform intensity along x, i.e, $I(x)=$constant, light rays emitted from the source toward direction β must intersect the CDOE at $x(\beta)$ [see Fig. 1(b)], obeying the relation

$$dx/d\beta = F\cdot S(\beta), \tag{9}$$

where the constant F is the paraxial focal length of the collimator, chosen to be much larger than the source size. Uniform diffraction efficiency was assumed in Eq. (9). $x(\beta)$ is obtained from Eq. (9) by integration, and $z(\beta)$ is simply given as

$$z(\beta) = x(\beta)/\tan\beta. \tag{10}$$

Hence the shape $z(x)$ of the uniform collimator CDOE is obtained.

As an example, consider the simplest case, of an isotropic "1D" light source (e.g., a line source or a diffuse cylindrical source) where $S(\beta)=$constant. The shape of the uniform collimator CDOE for this case, derived from Eqs. (9) and (10), is

$$z(x) = x/\tan(x/F). \tag{11}$$

Equation (11) is defined for the entire angular distribution $-\pi\leqslant\beta<\pi$, where $-\pi F<x<\pi F$ and $-\infty<z\leqslant F$, and therefore uniformly collimates the entire source energy. Part of $z(x)$ of Eq. (11) is shown in Fig. 3(a). As shown, the rays originating from the point source at equal angular density also have uniform spatial density along x, after collimation. On the other hand, when such rays are collimated by a PM [whose shape is $z(x)=F-x^2/(4F)$] the resulting spatial density along x is nonuniform, as seen in Fig. 3(b). Figure 4 shows the intensity profile $I(x)$ of the collimated beam for the CDOE and the PM. For the PM the intensity of the col-

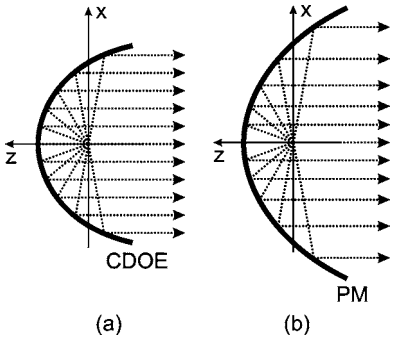

FIG. 3. Sections of two collimator shapes for an isotropic source (illustrated by a uniform angular density of emerging rays) with the same paraxial focal length: (a) a CDOE described by Eq. (11) for which collimated rays are equally spaced, indicating uniform intensity of the collimated beam; (b) a PM for which the spacing between collimated rays increases for larger x, indicating a reduction in intensity.

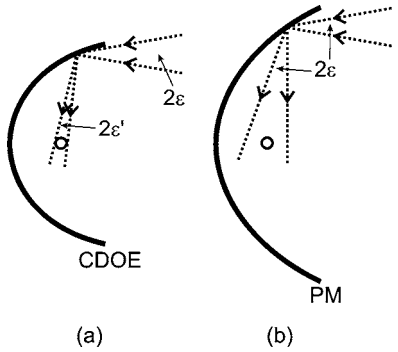

FIG. 5. Diffuse light concentration onto a small cylindrical target by: (a) a uniform collimator CDOE and (b) a PM. For the PM the reflected ray pencils have the same angular spread as the incoming ray pencils, resulting in poor concentration for large β. For the CDOE, for $\beta \neq 0$ the diffracted ray pencils are narrower than the incoming ray pencils ($2\varepsilon' < 2\varepsilon$), resulting in ideal concentration for all β.

limated beam satisfies $I(x) \propto 4/((x/F)^2+4))$, having a maximum at $\beta=0(x=0)$ and dropping monotonically to zero for $\beta=\pm\pi(x=\pm\infty)$, whereas for the CDOE $I(x)$=constant for all β. It can be seen that the CDOE shape—as was noted above—is limited between $-\pi < x/F < \pi$, whereas for the PM, $-\infty < x/F < \infty$, and that the entire collimated energy $\int_{-\infty}^{\infty} I(x)dx$ is the same for the two cases. Note that similar conclusions can be reached for a CDOE that satisfies design Eqs. (9) and (10), but works in transmission, instead of reflection.

Next, we consider the finite angular spread of the collimated beam resulting from a diffuse source with finite size. Here the goal is to design a collimator with a minimum angular spread for a given source size. Alternatively, when the direction of the rays is simply reversed, this goal is equivalent to designing a concentrator that will concentrate a uniform incoming diffuse beam on the smallest target of the given shape.

The Appendix presents an analytic proof that a CDOE that fulfills Eqs. (9) and (10) to collimate light uniformly for a given light source shape is inherently also an ideal diffuse light concentrator (collimator) for small diffusive angles and the same shape as a target (source) operating at the thermodynamic limit [Eqs. (5) and (6), respectively]. For example, the CDOE of Fig. 3(a), designed for uniform collimation for a line source, is also an ideal collimator for small cylindrical sources and an ideal diffuse light concentrator onto cylindrical targets. In the concentrator application the ray directions

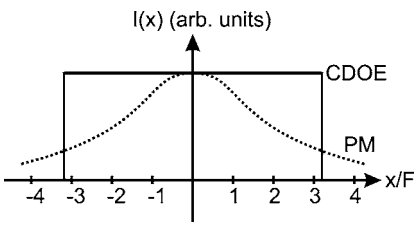

FIG. 4. Calculated intensity distributions for the collimated beam produced by a uniform collimator CDOE (solid line) and a PM (dotted curve), showing a uniform collimated intensity in the case of the CDOE and a nonunifom intensity in the case of the PM (as shown schematically in the ray diagrams in Fig. 3).

of Fig. 3(a) are simply reversed, and the target is placed in the focus so that its center coincides with the focal point.

Intuitively, this striking result can be understood by noting that the phase space density on the surface of a Lambertian source is uniform. Furthermore, the uniform intensity of the collimated beam [ensured by Eq. (9)] combined with its uniform diffusivity (shown in the Appendix to exist) indicate that the phase space density of the collimated beam is also uniform. Since linear optical transformations conserve the local phase space density, the total phase space area in a transformation between two uniform phase space distributions must be conserved. Moreover, this intuitive argument predicts that the amount of nonuniformity generated by the transformation of an initially uniform phase space distribution can be quantitatively related to the amount of increase in phase space area (and hence to the amount of decrease in brightness). We verified that indeed such a relation quantitatively holds for all the examples presented throughout the article.

Figure 5(b) illustrates why a PM fails as an ideal diffuse-light concentrator for 1D concentration on a uniform cylindrical target. At each point on the PM the incident light cone with half angle ϵ is reflected as an identical cone toward the focus. As $|\beta|$ approaches π, the distance from the reflection point to the focal point approaches infinity, and hence the spread of the reflected light cone at the focus also approaches infinity, resulting in a dramatic decrease in concentration performance. On the other hand, for the uniform CDOE collimator, as $|\beta|$ approaches π, the diffracted light cones are actually much narrower than the incident light cones ($\epsilon' \ll \epsilon$), as illustrated in Fig. 5(a), and exactly compensate for the increased distance to form a spot at the focus which is independent of β. Expansion of the diffraction relations of the grating for small ϵ and simple algebra yield for the CDOE that the extreme incident rays at angles $\pm\epsilon$ from the z axis are directed exactly tangent to the target, and all intermediate rays hit the target for all β.[6] These considerations are similar to the edge-ray principle used originally for the design of nonimaging concentrators[16] and discussed in Sec. II. Figure 6 presents the calculated normalized 1D concentration ratio onto a cylindrical target, as a function of $|\beta_{\max}|$

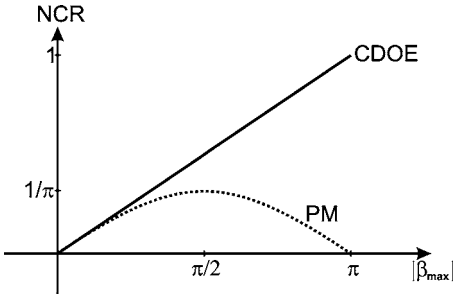

FIG. 6. Calculated normalized concentration ratio onto a small cylindrical target as a function of $|\beta_{\max}|$ for the uniform collimator CDOE (solid line) and the PM (dotted curve) with incoming half-diffusive angle $\epsilon < 5°$, indicating that the CDOE reaches the thermodynamic limit of concentration for $|\beta_{\max}| \to \pi$, whereas the optimum performance of the PM is $1/\pi$ worse than the thermodynamic limit.

for both the uniform-collimator CDOE and the PM. It can be easily shown that for the CDOE the normalized concentration ratio is $|\beta_{max}|/\pi$, which yields concentration at the thermodynamic limit for $|\beta_{\max}| = \pi$. For the PM the normalized concentration ratio is $\sin|\beta_{\max}|/\pi$, resulting in an optimal concentration at $|\beta_{\max}| = \pi/2$, the maximum concentration ratio being π times below the thermodynamic limit.

The design procedure of Eqs. (8)–(10) was verified experimentally[6] by holographically recording a reflection CDOE of the shape given by Eq. (11) [and shown in Fig. 3(a)]. The focal length of the CDOE was $F=20$ mm. Several consecutive exposures were used to record a hologram for the range $-\pi/2 \leqslant \beta \leqslant \pi/2$ [corresponding to numerical aperture (NA)=1 and a lateral size of $2x_{\max}=58$ mm]. Since a spherical (instead of a cylindrical) wave was used for the recording, a 5 mm slit in the y direction ensured that the setup worked essentially as a 1D concentrator. To test the performance of the uniform collimator CDOE as an ideal concentrator, the setup shown in Fig. 7 was used. The entire aperture of the CDOE was illuminated with a monochromatic plane wave that was inclined at variable angle ϵ with respect to the z axis. A cylindrical black target (T) with radius $r=1.5$ mm at the focal point of the CDOE should block all the concentrated light when $|\epsilon| \leqslant r/F = 4.3°$ and none of it for $|\epsilon| > 4.3°$ for an ideal concentrator. The unblocked light power was measured by integrating the unblocked light intensity that hit a white diffuse screen (S) placed behind the target. The measured unblocked power graph, shown in Fig. 8 with diamonds, features a discontinuous sharp transition close to $\epsilon = r/F = 4.3°$, indicating near-ideal concentration. The theoretical unblocked power curve for the CDOE concentrator, obtained from numerical ray tracing (Fig. 8, solid line) has a somewhat sharper, but still finite slope. This nonideal concentration is due to the finite size of the target, corresponding to a finite input diffuse angle, and is further studied in the next paragraph. Finally, the theoretical unblocked power curve for the PM concentrator (Fig. 8, dashed line) has a much softer slope, indicating concentration well below the thermodynamic limit.[6]

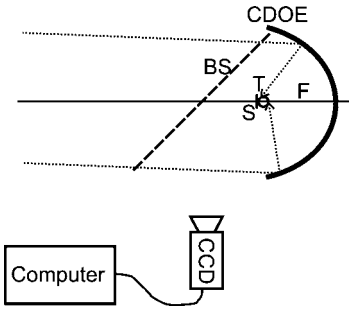

FIG. 7. Setup for measuring the concentrating performance of the uniform collimator CDOE. The CDOE is illuminated with a monochromatic plane wave inclined at variable angle ϵ with respect to the z axis. A cylindrical black target (T) is placed at the focal point of the CDOE and the unblocked light intensity is measured by integrating the unblocked light intensity that hits a white diffuse screen (S) placed behind the target and imaged with the help of a beam splitter (BS) onto a calibrated CCD camera.

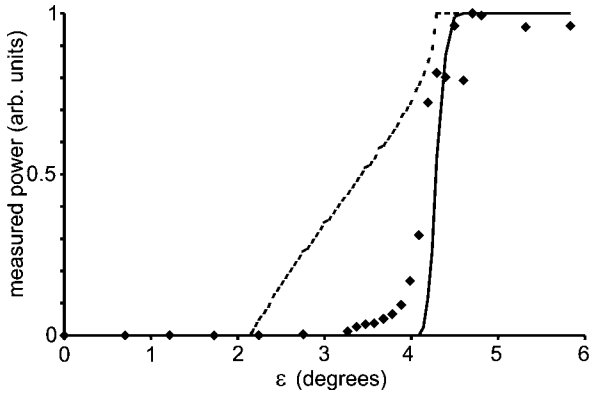

FIG. 8. Experimental data for characterizing the performance of the uniform collimator CDOE as a diffuse light concentrator onto a small cylindrical target, obtained using the setup of Fig. 7. The measured light intensity not blocked by the cylindrical target as a function of the illumination angle (diamonds) shows good agreement with the theoretical calculations for the CDOE (solid curve). Also included is the theoretical graph for the PM (broken curve), showing poor performance of the PM as a diffuse light concentrator. Note that any measured intensity below the ideal cutoff angle of 4.3° results from nonideal concentration.

Since the edge ray principle for CDOEs is derived (in the Appendix) using the diffraction relation for infinitesimal diffusive angles, it is only an approximation for large diffusivities. The effect of noninfinitesimal diffusivities was numerically investigated for the concentrator CDOE shape of Fig. 3(a). Two cases were considered: when $|\beta_{\max}| = 90°$ (corresponding to the optimal geometry for the PM) and $|\beta_{\max}| = 140°$. In the latter case the maximum diffusivity that can be considered was calculated to be limited to a total divergence angle of $2\epsilon_{\max} = 16°$ by the requirement to avoid shadowing effects. The numerical results are presented in Fig. 9. The vertical axis represents the efficiency of the CDOE as an ideal concentrator, defined as the fraction of the incoming light intensity that hits the target having the thermodynamic-limited radius of $F \cdot \sin \epsilon$. As seen in Fig. 9, the CDOE shape obtained from the design Eqs. (9) and (10) has nearly ideal concentration even for large diffusivities. For example, for $2\epsilon_{\max} = 0.5°$, similar to the diffusivity of solar light, the concentration efficiency is 99.8% at $|\beta_{\max}| = 140°$ and 99.9% at $|\beta_{\max}| = 90°$. Even for $2\epsilon_{\max} = 16°$ the concentration efficiency is 96% at $|\beta_{\max}| = 140°$ and 98% at $|\beta_{\max}| = 90°$. For comparison, the corresponding efficiencies for a PM concentrating on the same cylindrical target (not shown in Fig. 9) are 44% at $|\beta_{\max}| = 140°$ and 79% at $|\beta_{\max}| = 90°$. In the design of spe-

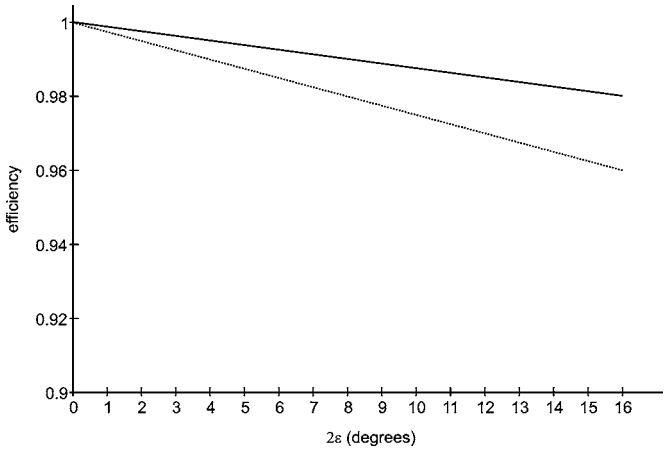

FIG. 9. The effect of noninfinitesimal diffusive angles on the concentration efficiency of the uniform collimator CDOE, obtained from numerical calculations for two cases: for $|\beta_{max}|=90°$ (corresponding to the optimal geometry for the PM) and $|\beta_{max}|=140°$. The CDOE has nearly ideal concentration even for large diffusivities.

cific practical systems, similar numerical analyses can also be conducted to incorporate other deviations from the ideal case. These include the less than 100% (and possibly space-variant) diffraction efficiency of the CDOE, and the finite bandwidth (e.g., for a LED, $\Delta\lambda/\lambda \sim 2\%–3\%$) and spectral distribution of the applied light source.

Naturally, the design procedure for a uniform collimator described by Eqs. (9) and (10) can be applied for more general Lambertian source shapes. Figure 10 demonstrates a few examples that yield simple analytic solutions for the uniform collimator CDOE shape: a vertical flat source radiating from one side (solid curve) and a horizontal flat source radiating from two sides (dashed curve), corresponding to CDOE shapes of $z(x)=\sqrt{F^2-x^2}$ and $z(x)=|x|\cdot(F-|x|)/\sqrt{2F|x|-x^2}$, respectively. For comparison, the CDOE for an isotropic source is also shown in Fig. 10 [dotted curve, the shape of Fig. 3(a) and Eq. (11)]. The CDOE shape for a one-sided flat source—which is exactly the half cylinder that satisfies the Abbe sine condition—is significant for many practical cases, and will be discussed in detail in Sec. V. Equations (9) and (10) yield simple analytic solutions for the CDOE shapes with Lambertian sources having elliptical, square, triangular, and many other cross sections.[6]

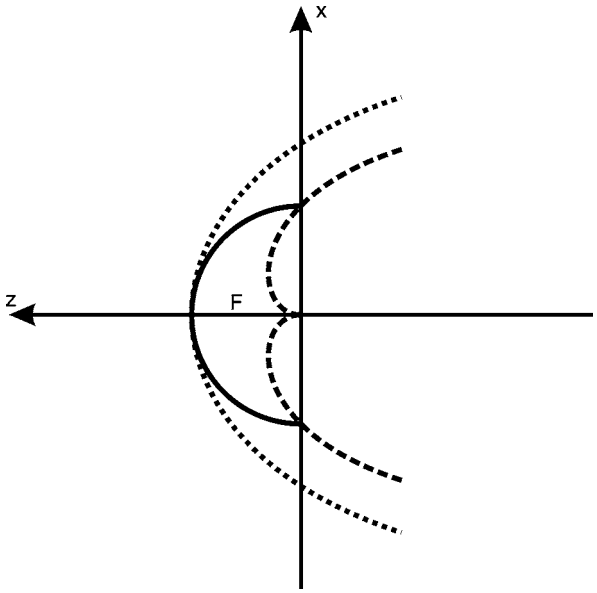

FIG. 10. Uniform collimator CDOE profiles for small Lambertian sources of different shapes located at $x=0$, $z=0$. The CDOE profiles correspond to the following source shapes: one sided (vertical) flat source (solid curve), double sided (horizontal), flat source (dashed curve), and isotropic source (dotted curve). All CDOEs have the same paraxial focal length F and extend to $-\pi<\beta<\pi$ (except for the one sided flat source which is limited to $-\pi/2<\beta<\pi/2$).

Finally, the design procedure of the CDOE presented in this section [Eqs. (8)–(10)] is not limited to uniform collimation, but can also be used to form other desired light intensity profiles of the collimated beam. For example, for a collimated beam with a Gaussian intensity distribution $I(x) \propto \exp(-x^2/x_0^2)$ the CDOE shape is $\beta(x) \propto \mathrm{erf}(x/x_0)$, where erf is the error function, i.e., the integral of the Gauss function. For this case the CDOE shape looks somewhat like a parabola, which is not surprising, considering that a parabolic mirror yields a nearly Gaussian collimated intensity profile (see Fig. 4). In this regard, CDOEs may also be used to change the intensity distributions of a collimated beam. For example, a configuration for transforming a collimated Gaussian beam into a collimated uniform-intensity beam, also based on a CDOE, is presented in Ref. 13.

IV. IDEAL CONCENTRATION IN 1D WITH CDOEs AT FINITE DISTANCE

The design principle described in Sec. III can be implemented and generalized for finite distances between the source and the target,[18] both for reflection and transmission geometries in one dimension. The problem to be solved can be stated as follows: the light from an elongated Lambertian source of given size and cross-sectional geometry is to be uniformly concentrated onto an elongated target of given cross-sectional shape and the minimal cross-sectional size that is permitted by the thermodynamic limit. This general problem has great practical significance, e.g., for the side pumping of solid-state laser rods, where high geometrical efficiency and uniform pump density profile are important. Existing laser pump cavities, based on conventional elliptical mirrors (with the laser rod located in one focus of the ellipse and the pumping lamp located at its other focus), do not yield uniform pumping even if the pump lamp emits light uniformly. This nonuniformity is also translated into light concentration below the thermodynamic limit, as shown in Sec. III for the infinite distance case.

As in Sec. III, since we consider parallel, elongated sources and targets, only rays in the transverse directions are important for the design, hence a 2D Cartesian coordinate system can be used.

First consider a reflection CDOE. Figure 11(a) shows schematically the design geometry for a reflection CDOE for 1D diffuse-light concentration at finite distance. A small source is centered at point A and a small target is located at a distance d, centered at point B. The source emits radiation with angular (far-field) intensity distribution $S_1(\alpha)$, where α is the angle between the direction of the radiation and the

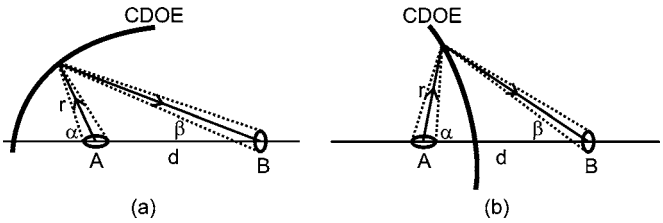

FIG. 11. Design geometry of a CDOE for concentration at finite distance working in: (a) reflection and (b) transmission. Source A and target B are at a distance d from each other, α is the angle between a central ray emitted by A and the line connecting A and B, β is the angle between the central ray intercepted by B and the line connecting A and B, and r is the distance between A and the given point on the CDOE.

line connecting A and B. As discussed in Sec. III and shown in Fig. 2, for general 2D Lambertian sources $S_1(\alpha) \propto \Delta_1(\alpha)$, where $\Delta_1(\alpha)$ is the projected diameter of the source as seen from direction α. Similarly, $S_2(\beta)$ is the local intensity of the output beam in direction β, measured at the target, as shown in Fig. 11(a). From energy conservation we get:

$$S_1(\alpha)d\alpha = S_2(\beta)d\beta. \tag{12}$$

To ensure uniform illumination on a Lambertian target, $S_2(\beta)$ must be proportional to $\Delta_2(\beta)$, where $\Delta_2(\beta)$ is the projected diameter of the target as seen from direction β. Hence for Lambertian source and target, Eq. (12) takes the form

$$\Delta_1(\alpha)d\alpha = \Delta_2(\beta)d\beta. \tag{13}$$

The CDOE shape $r(\alpha)$ for specific $\Delta_1(\alpha)$ and $\Delta_2(\beta)$ geometries of the source and the target, respectively, is obtained by solving differential Eq. (13) for β, and then substituting it into the relation

$$r(\alpha) = \frac{d \cdot \sin\beta(\alpha)}{\sin[\alpha - \beta(\alpha)]}, \tag{14}$$

as seen in Fig. 11(a). The meaning of d as the scaling parameter is similar to that of F in Eq. (9).

This design principle together with Eqs. (12) and (13) is also valid for the geometry of a transmission CDOE concentrator, presented in Fig. 11(b). However, since here α is measured from the opposite direction, Eq. (14) is modified to

$$r(\alpha) = \frac{d \cdot \sin\beta(\alpha)}{\sin[\alpha + \beta(\alpha)]}. \tag{15}$$

As for the uniform collimator CDOE described in Sec. III, again by expanding the diffraction relations of the holographic grating for small diffuse angles (i.e., when the source and target sizes are much smaller than d) we prove analytically in the Appendix that for the CDOE designs of Eqs. (13)–(15) the rays emitted tangentially by the source are directed exactly tangent to the target, and hence all intermediate rays emitted by the source hit the target for all α. Moreover, the phase-space area is conserved, i.e., $(\text{phase-space area})_{\text{target}} = (\text{phase-space area})_{\text{source}}$. Therefore, if there is no loss in power, such a device concentrates diffuse light at the thermodynamic limit, i.e., on the smallest possible target size of the given geometry. The experimental realization of such a holographic element is quite simple, since the curved hologram can be recorded using two simple cylindrical laser beams, originating from locations A and B [see Figs. 11(a) and 11(b)].

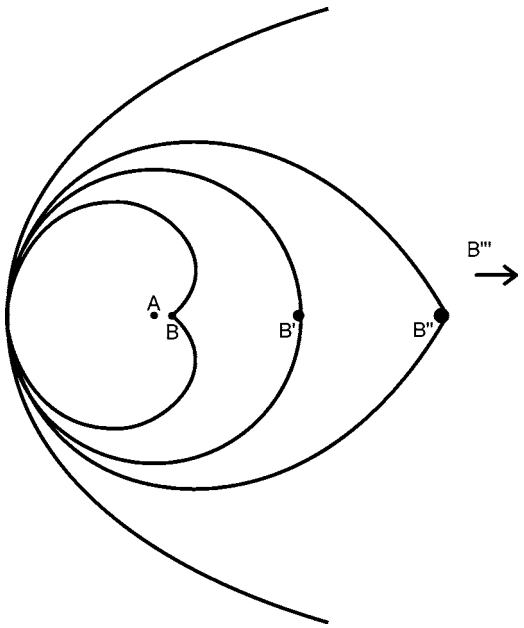

FIG. 12. CDOE profiles for a cylindrical source A and cylindrical targets of different sizes B, B', B'', and B'''. The corresponding magnifications are $M=1.1$, 2, 3, and ∞, respectively. The CDOE shape corresponding to $M=\infty$ is the uniform collimator/concentrator shown in Fig. 3(a).

As the first example of a CDOE designed from Eqs. (13) and (14), consider a cylindrical source emitting rays with uniform angular distribution in the entire angular range $-\pi \leqslant \alpha < \pi$, and a target that receives rays with uniform angular distribution in the limited angular range $(-\pi/M) \leqslant \beta < (\pi/M)$, where M is the linear magnification of the CDOE. (The role of source and target can, of course, be interchanged, and then M becomes demagnification). Here both $\Delta_1(\alpha)$ and $\Delta_2(\beta)$ are constants, and Eq. (13) yields $d\alpha = Md\beta$. The solution is $\beta = \alpha/M$, and from Eq. (14) we get $r(\alpha) = d \cdot \sin(\alpha/M)/\sin\{(1-1/M)\alpha\}$. Several shapes, corresponding to $M=1.1$, 2, 3, and ∞, and targets B, B', B", and B"', respectively, are shown in Fig. 12. The CDOE shape corresponding to $M=\infty$ is the uniform collimator/concentrator discussed in Sec. III and shown in Fig. 3(a). The CDOE shape corresponding to $M=2$ is a simple cylinder $[r(\alpha)=d=\text{constant}]$, where A is at the center and B is on the circumference. As $M \to 1$, the CDOE cross-sectional shape approaches the so-called cochleoid curve, for which $r(\alpha) \propto \sin\alpha/\alpha$. The $M<\infty$ cases of the CDOE shapes can be applied to direct the rays coming from a cylindrical source onto a cylindrical target, where the diameter of the target is M times larger than the diameter of the source.

Figure 13 (dashed line) presents the calculated uniformity of the CDOE concentrator, i.e., the spot size of the beam on the target as a function of α. Also shown in Fig. 13 are several corresponding calculated graphs for the same cylindrical source illuminating reflective elliptical cavities having various eccentricities e (solid curves). Here the source is placed at one focal point of the elliptical mirror and the target at the other focal point. As seen in Fig. 13, the different portions of the CDOE all yield the same spot size at the

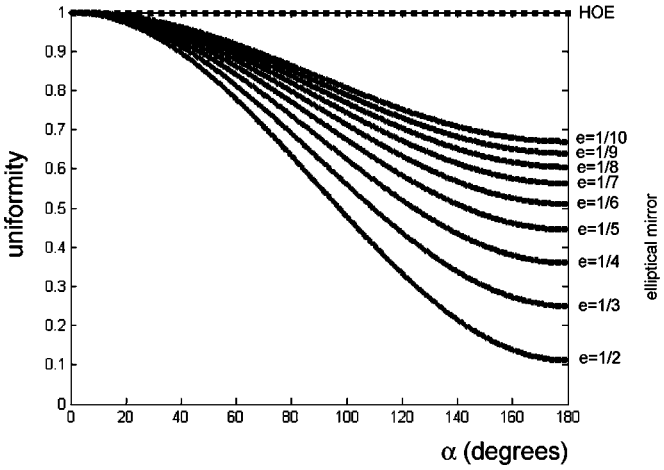

FIG. 13. Calculated normalized spot sizes as a function of α for a CDOE (dotted line) and for reflective elliptical cavities having different eccentricities e (solid curves), indicating that the CDOE yields a uniform intensity distribution on the target, whereas the concentration profiles of the elliptical cavities are highly nonuniform.

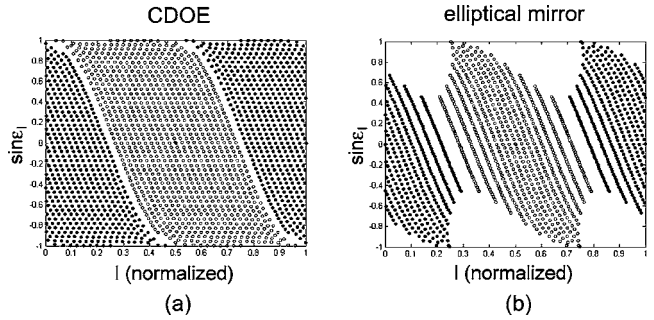

FIG. 15. Phase-space spot diagrams obtained from numerical ray tracing at the cylindral target of: (a) the double CDOE cavity of Fig. 14(a), and (b) the double elliptical mirror cavity of Fig. 14(b). Rays coming from the left side source and the right side source are represented by filled circles and open circles, respectively. The double CDOE device has a much more uniform phase space than the double elliptical mirror, and achieves uniform concentration at the thermodynamic limit.

target's location, whereas the spot sizes created from different portions of the elliptical mirror are highly nonuniform. In fact, for the elliptical mirror the ratio between the minimum and maximum spot sizes is $[(1-e)/(1+e)]^2$. Note that as $e \rightarrow 0$, the uniformity achieved by the ellipse slowly converges to 1. However, this case corresponds to a nearly circular mirror cross section of extremely large size compared with the source-target distance. Since uniform pump-density profile, besides high pumping efficiency, is often desirable in a laser rod, especially when fundamental transverse modes are to be excited, the CDOE may give a practical alternative to elliptical reflector tubes as pump cavities for solid state lasers.

Figure 14(a) shows how, for example, two CDOEs with $M=2$ can be used in a double lamp configuration in the pumping of solid-state lasers. The two cylindrical pump lamps are located in the center of the two cylindrical CDOEs, and the axis of the cylindrical laser rod coincides with the straight line where the two CDOEs touch. To avoid shadowing effects, neither of the two CDOEs is completely closed, as shown in Fig. 14(a). This leads to a small geometrical loss in power, since some of the rays emitted by the sources do not reach the CDOE. However, if the source and the target sizes are made much smaller than the DOE cross-sectional size, this geometrical loss becomes negligible. Since the magnification of both CDOEs is $M=2$, the combined phase-space area of the two sources is expected to be equal to the phase-space area of the target. To summarize, the double CDOE configuration of Fig. 14(a) conserves brightness and provides a uniform pump density profile. For comparison, Fig. 14(b) shows a double elliptical pumping configuration, which is used for solid state lasers. In order to provide the same magnification $M=2$ (and hence phase-space area conservation) as in the CDOE case, an eccentricity of $e=1/3$ was chosen for both ellipses. As seen in Fig. 14(b), combining the two ellipses causes relatively large portions of both mirrors to be missing, and hence a large percentage of the rays emitted by the sources does not arrive at the proper elliptical mirror surface and is essentially lost. The inherent geometrical loss in this case is $\sim 30\%$, which corresponds to an equal amount of loss in brightness.

As shown in Fig. 13, a drawback of elliptical cavities in general is their highly nonuniform pump density profile. This is further illustrated for the double elliptical cavity in Fig. 15. Figures 15(a) and 15(b) show phase space spot diagrams of rays hitting the cylindrical target, for the double CDOE and the double elliptical reflector, respectively, obtained from numerical ray tracing for the paraxial case (i.e., when the source and target sizes are much smaller than the size of the cavity). The horizontal axis l represents the location of the rays along the circumference of the target, and the vertical

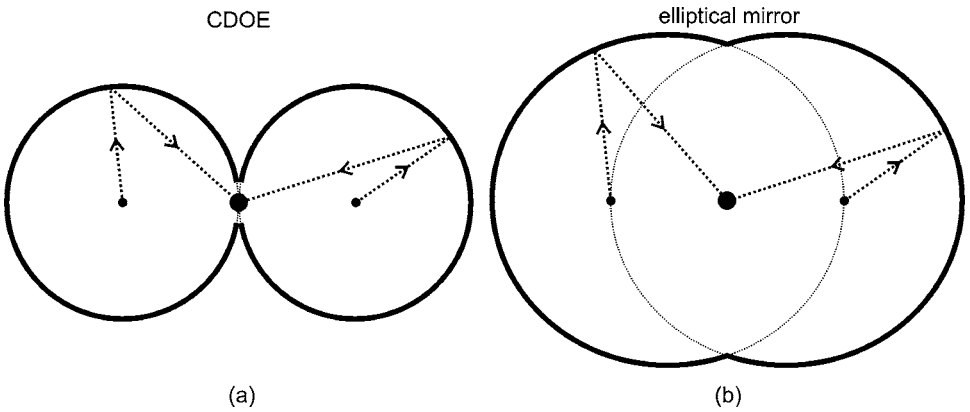

FIG. 14. Double lamp pumping configurations using: (a) two reflective CDOEs and (b) two reflective elliptical cavities. In this case the CDOEs have cylindrical shapes. The CDOEs yield smaller geometrical loss and a more uniform pump density profile than the elliptical cavities.

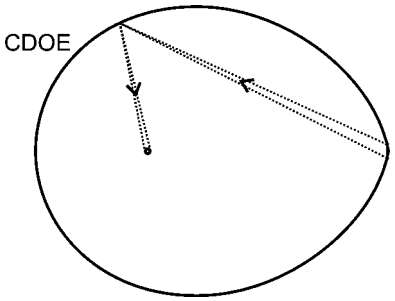

FIG. 16. Reflective CDOE concentrator shape designed using Eqs. (13) and (14) for a one sided flat Lambertian source and a cylindrical Lambertian target, having practical significance, e.g., for the side pumping of cylindrical solid-state laser rods with laser diode arrays that have a flat radiating surface.

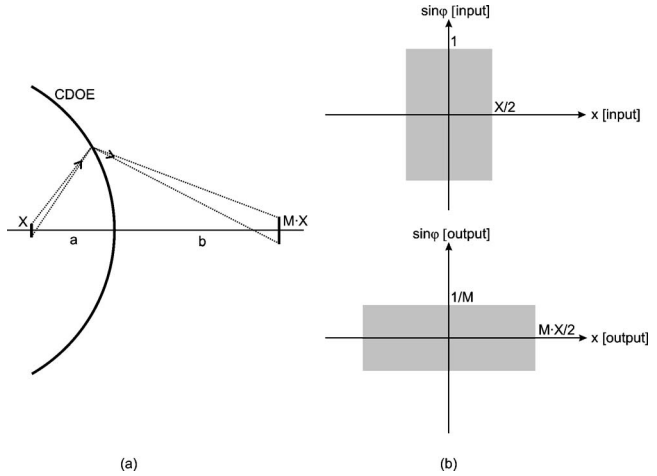

FIG. 17. (a) Transmission CDOE concentrator shape satisfying the Abbe condition with magnification M, and (b) phase-space diagrams of the light distributions at the input (source) and output (target), where x is the location of a particular ray on the source/target, and φ is its inclination angle of the ray from the optical axis. Although the target size is M times as large as the source size, the sine of the angular range of rays hitting the target is $1/M$ times as large as the sine of the angular range of rays emitted by the source, hence phase-space area is conserved.

axis represents the sine of the angle ϵ_1 between the rays and the surface normal. The density of dots at any region on the phase space diagrams gives directly the local brightness of light in that region. The rays are emitted isotropically from the sources, half from the left source (full circles in Fig. 15) and half from the right source (empty circles). Figure 15(b) is found to contain only ~70% of the illuminating dots, in agreement with the geometrical loss calculated above. As also seen, the phase space of the double elliptical reflector is highly nonuniform and contains empty regions. On the other hand, the double CDOE configuration yields uniform phase-space density, and light concentration at the thermodynamic limit.

We note that in practical laser pump cavities the size of the source and target are often comparable to the distance d between them. Also, multiple reflections from the walls are often used to further increase the probability of pump photons to be absorbed by the laser rod. Such practical complications can change the results obtained for the simple case considered here.

Figure 16 shows another CDOE design, using Eqs. (13) and (14) to concentrate light from a one-sided flat Lambertian source onto a cylindrical Lambertian target. This device may have practical significance for the side pumping of cylindrical solid-state laser rods with laser diode arrays that have a flat radiating surface. Naturally, the same CDOE shape corresponds to the case when the source and the target are interchanged.

For the special case of a flat Lambertian source and a flat Lambertian target Eq. (13) takes the form $\cos\alpha\, d\alpha = M\cos\beta\, d\beta$, which gives back exactly the Abbe condition $\sin\alpha/\sin\beta = M$, and the CDOE shape is a cylinder with radius $R = ab/(a+b)$, where a and b are the distances of the source and the target from the CDOE, respectively (both a and b follow the sign convention of being positive when they are to the left of the CDOE and negative when they are to the right), and $M = -b/a$. Such a CDOE working in transmission and at $M=2$ is presented in Fig. 17(a). Phase-space area conservation can be proved for this case by noting that although the target size is M times as large as the source size, the sine of the angular range of rays hitting the target is exactly $1/M$ times as large as the sine of the angular range of rays emitted by the source, as shown on the phase-space diagrams of Fig. 17(b), where x is the location of a particular ray on the source/target, and φ is the inclination angle of the ray from the optical axis. For $M=1$ the radius of the cylinder becomes infinity (corresponding to a flat DOE, placed halfway between the source and the target), and for $M\to\infty$ the circle is centered at point A. Such CDOEs satisfying the Abbe condition are very relevant for many applications and will be discussed in detail in the next section.

V. CDOEs SATISFYING THE ABBE CONDITION

A. The Abbe condition

For an imaging system, the Abbe condition[1] states that first-order aberrations (i.e., aberrations that grow linearly with the distance of the object point from the optical axis) are eliminated if

$$\frac{\sin\alpha}{\sin\beta} = \text{constant} = -\frac{b}{a}, \tag{16}$$

where α and β are arbitrary angles of the input and the output rays that connect an on-axis object point to an on-axis image point, and a and b are the object distance and the image distance (taken to be positive when they are to the left of the imaging system and negative when they are to the right), respectively. A system that satisfies the Abbe condition Eq. (16) is called aplanatic. The surface that satisfies condition (16) was shown[19] to be a sphere—or in 2D geometry, a cylinder—with radius

$$R = ab/(a+b). \tag{17}$$

Hence, if a CDOE is located on such an Abbe surface (a cylinder or a sphere), it is free of first-order aberrations for off-axis points at an object distance a and an image distance b.

B. Aplanatic CDOEs for concentration and collimation of diffuse light

Solving the CDOE design Eqs. (13)–(15) for 1D concentration from a flat Lambertian source onto a flat Lambertian target yields a cylindrical CDOE whose radius exactly satisfies Eq. (17). This is not surprising, since for an imaging system the Abbe condition applies for the case in which both the object and the image are located on flat surfaces perpendicular to the optical axis. Furthermore, since aplanatic CDOEs eliminate aberrations that grow linearly with the size of the object (the source) and the image (the target), CDOEs satisfying the Abbe condition work as ideal concentrators between flat sources and targets for small source and target sizes.

Such an aplanatic CDOE was investigated theoretically and experimentally for diffuse light concentration.[20] For the experiments a 6 cm wide cylindrical reflective CDOE with radius $R=3.5$ cm and $\mathrm{NA}=3/3.5=0.86$ was recorded, using a plane wave and a counterpropagating spherical wave whose center coincided with the center of the cylinder (see Fig. 1). The spherical and plane waves were derived from an argon-ion laser operating at a wavelength of 488 nm. The recording material was a 20 μm thick photopolymer which was glued to a thin glass half cylinder. After exposure and development the resulting CDOE had a diffraction efficiency of $\sim 70\%$, with uniformity better than $\pm 10\%$ over the entire aperture.

For comparison, a flat DOE was also recorded with the same parameters. The flat DOE had the same length (6 cm) and focal distance (3.5 cm) as the CDOE, but its NA $[=\sin(\tan^{-1}(3/3.5)=0.65]$ is smaller than that of the CDOE. Note that with several consecutive recordings $\mathrm{NA}=1$ is easily achievable for the CDOE.[6] The CDOE and the flat DOE were illuminated with diffuse light. The diffuse source was simulated by passing a uniform beam from an argon laser with a wavelength of 488 nm through a rapidly rotating diffuser located at the back focal plane of a lens. A variable aperture placed adjacent to the rotating diffuser was used to control the diffusive angle. A horizontal slit of about 1 cm width ensured that the setup worked essentially in one dimension (alternatively, the microscope objective used during recording could have been replaced with a cylindrical lens).

The concentrated spot was obtained on a 5 mm wide screen located at the focal plane of the CDOE or flat DOE, and imaged onto a calibrated charge coupled device (CCD) camera. Some representative experimental concentrated spots are shown in Figs. 18(a) and 18(b) for the CDOE and the flat DOE, respectively. The relevant parameters for the results were as follows: element aperture=6 cm, focal length=3.5 cm, and half-divergence angle $\epsilon_x=1°$ (much smaller than the Bragg selectivity angle of the DOEs, to ensure high diffraction efficiency). The corresponding horizontal intensity cross sections are shown in Fig. 19(a). As seen, the CDOE yielded a narrower spot than the flat DOE, with clearly observable sharper edges. The results for the corresponding calculated intensity cross sections—obtained from numerical ray tracing—are presented in Fig. 19(b), and are seen to be in good agreement with the experimental ones. These measurements were repeated as a function of NA for the two DOEs. The NA was varied by placing an aperture with variable width adjacent to the DOEs that limited their effective size.

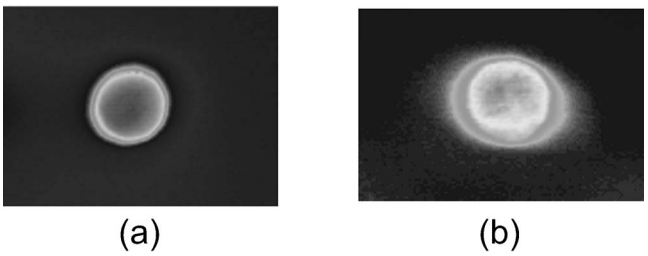

FIG. 18. Experimental concentrated spots on a flat target obtained from: (a) a cylindrical aplanatic CDOE and (b) a flat DOE. For both cases the DOEs have an aperture of 6 cm, and a focal length of 3.5 cm. A diffuse beam with half-divergence angle $\epsilon_x=1°$ is used for the illumination.

From the horizontal spot sizes the 1D normalized concentration ratio was calculated. The results are shown in Fig. 20, with *O*s and *X*s for the CDOE and the flat DOE, respectively. Also shown in Fig. 20 are the calculated normalized concentration ratios for the CDOE (solid curve), the flat DOE (dotted curve), and the PM (dashed curve), having the analytical expressions of NA, $\mathrm{NA}\cdot(1-\mathrm{NA}^2)$, and $\mathrm{NA}\cdot(1-\mathrm{NA}^2)^{1/2}$, respectively. As seen, the maximum achievable concentration ratio for the PM and the flat DOE is 50% (at $\mathrm{NA}=0.71$) and 38% (at $\mathrm{NA}=0.58$) of the thermodynamic limit, respectively. For 2D concentration (discussed in more detail in Sec. VI) the best normalized concentration ratio for the PM and the flat DOE is even lower, namely 25% and 15%, respectively, of the thermodynamic limit, whereas for the CDOE, concentration at the thermodynamic limit is still achieved.

The aplanatic CDOE thus has the advantage of ideal concentration of diffuse light onto a flat target at the thermodynamic limit. Additionally, it is very simple to fabricate since a cylindrical/spherical substrate and only readily available cylindrical/spherical and plane waves are needed for the recording. However, in order to reach high diffraction efficiency, Bragg CDOEs, or blazed surface-relief CDOEs should be used for concentration. In this case the angular selectivity of the CDOE puts an upper limit on the usable input diffusive angle ϵ_x. ϵ_x is also limited by higher-order aberrations, which the aplanatic CDOE does not eliminate.

In a somewhat related approach, a curved refractive Fresnel lens was suggested for 1D concentration of sunlight.[21,22] Here the lens shape and the groove angle of the prismatic grooves can be calculated numerically—using a design principle similar to the edge ray principle—for a given ϵ_x and n, where n is the index of refraction. If n is small then the obtainable concentration ratio is much worse than the thermodynamic limit (e.g., by a factor of 2.6 for refractive index $n=1.1$ and by a factor of 1.33 for $n=1.5$, when the diffuse angle $\epsilon_x \to 0°$). The performance of the curved refractive Fresnel lens approaches that of the aplanatic CDOE in the limiting case of $\alpha_x \to 0°$ and $n \to \infty$, when the Fresnel lens has no grooves and can be treated as an aplanatic holographic CDOE.

Naturally, by reversing the direction of the light rays, the spherical/cylindrical CDOEs can also uniformly collimate

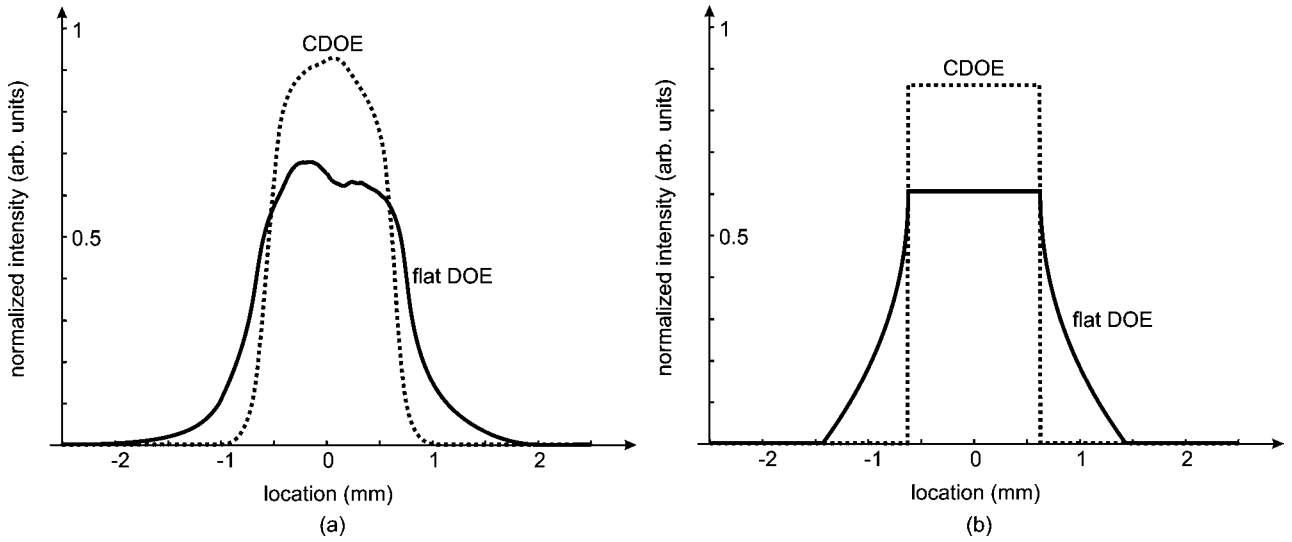

FIG. 19. (a) Measured horizontal intensity cross sections of the concentrated spots of Fig. 18 for the cylindrical aplanatic CDOE (dotted line) and the flat DOE (solid line), showing that the CDOE yielded a narrower spot with sharper edges than the flat DOE, and (b) the corresponding calculated intensity cross sections obtained from numerical ray tracing.

the light emitted from a flat Lambertian source into a uniform intensity beam with the smallest diffusivity consistent with the thermodynamic limit. This result is obtained as a special case from the uniform collimator design principle, presented in Sec. III for general Lambertian sources.

C. Aplanatic CDOEs for imaging

The aplanatic CDOE was suggested for aberration-free imaging by several authors.[14,19,23–33] The same cylindrical CDOE and flat DOE mentioned above for diffuse light concentration were also tested experimentally for imaging.[14] In this experiment, the two DOEs were illuminated with a collimated plane wave, rather than a diffuse beam. The off-axis angle ε of the illuminating plane wave was varied and the focused spots were imaged on a calibrated CCD camera. Figure 21 shows the measured horizontal spot sizes (defined as the region containing 90% of the total energy) of the flat DOE (squares) and the CDOE (diamonds), plotted as functions of ε. As seen, the CDOE has essentially a fixed spot size (limited here by the resolution of the CCD camera), whereas the flat DOE has large aberrations for large off-axis angles.

Since the aplanatic CDOE only eliminates aberrations that grow linearly with ϵ, while retaining higher-order aberrations, numerical ray tracing simulations are required to determine the overall effect of aberrations and to confirm the superiority of the CDOE over the flat DOE.[14] The results are shown in Fig. 22, which presents the ratio between Δ_F and Δ_C, the rms deviations of the output ray positions from the desired focal point, for the flat DOE and the CDOE, respectively. This ratio is plotted as a function of the NA for off-axis illuminating angles of $\varepsilon=2°$ (solid curve) and $\varepsilon=5°$ (dotted curve). As can be seen, the CDOE performs especially well compared with the flat DOE for moderate ε and

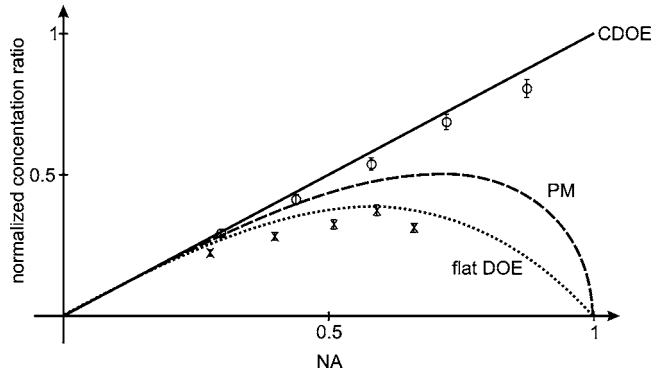

FIG. 20. Calculated normalized concentration ratio for the cylindrical aplanatic CDOE (solid line), the flat DOE (dotted line), and the PM (dashed line) as a function of NA. Also shown are the experimental normalized concentration ratio values for the CDOE (O) and the flat DOE (X), with error bars estimated from the data. The aplanatic CDOE reaches the thermodynamic limit at high NA, whereas the maximum achievable concentration ratio for the PM and the flat DOE is 50% (at NA=0.71) and 38% (at NA=0.58) of the thermodynamic limit, respectively.

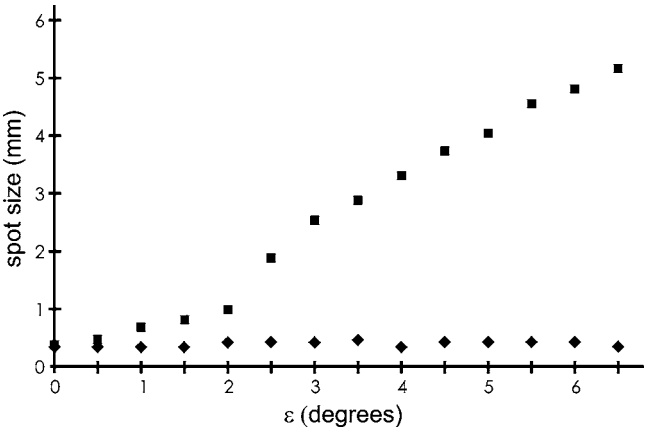

FIG. 21. Measured horizontal spot sizes (defined as the diameter of the region containing 90% of the total energy) of a cylindrical aplanatic CDOE (diamonds) and a flat DOE (squares), as a function of the off-axis angle ε of the illuminating plane wave. As seen, the flat DOE has large aberrations at large off-axis angles, whereas the CDOE has an essentially fixed spot size. For both cases the DOEs have an aperture of 6 cm, and a focal length of 3.5 cm.

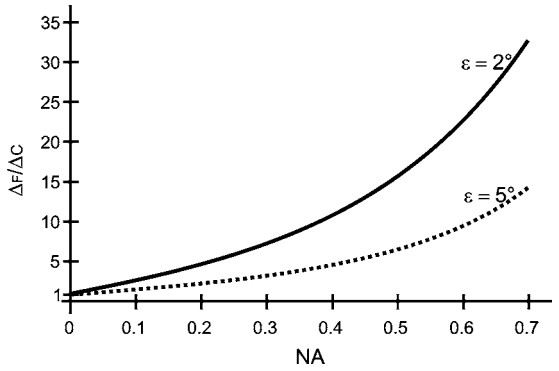

FIG. 22. The ratio between the combined aberrations Δ_F and Δ_C (defined as the rms deviations of the output ray positions from the desired focal point), for the flat DOE and the aplanatic CDOE, respectively, as a function of NA, for off-axis illuminating angles of $\varepsilon=2°$ (solid curve) and $\varepsilon=5°$ (dotted curve), obtained from ray tracing simulations. As seen, the CDOE performs especially well compared with the flat DOE for high NAs.

high NAs, e.g., yielding a significant ratio of $\Delta_F/\Delta_C=33$ for NA=0.7 and $\varepsilon=2°$.

In some cases, where a transmission CDOE is recorded holographically on the inner surface of a spherical/cylindrical meniscus substrate, the substrate may introduce both spherical aberration and coma.[24] By appropriately choosing the location of the two recording point sources and the location of the reconstructed image point, both aberrations can be cancelled.[24] If the two radii of the meniscus substrate are free parameters, then they should be chosen such that the inner and outer meniscus surfaces have a common center of curvature which coincides with the focal point of the CDOE.[25] This geometry ensures that the finite thickness of the substrate does not introduce appreciable aberrations in the system.

A special application of CDOEs was reported for planar optics.[33] Because of the plane geometry, astigmatism does not exist, and the only low-order aberrations that should be corrected in such an imaging system are spherical aberration, coma, and field curvature. Spherical aberration and coma can be simultaneously eliminated by a circular CDOE which satisfies the Abbe condition and by appropriate choice of the phase function on the CDOE.[7] For example, an aplanatic planar Fresnel lens can act as the CDOE.[33] Since an aplanatic Fresnel lens and an aplanatic refractive lens have field curvatures of opposite sign, they can be combined to form a hybrid system that eliminates field curvature too, and hence is completely free of all low-order aberrations.[33]

We only mention briefly here that for general—not necessarily aplanatic—spherical CDOEs that are recorded and reconstructed with spherical waves, detailed higher-order aberration analysis was done by several authors.[26–31] These studies were reviewed in detail elsewhere[7] and only a few results are mentioned here. In certain cases the entrance pupil of the focusing system is located at a distance from the CDOE, and the location of the entrance pupil, along with the radius of the CDOE, provide free parameters for numerical optimization.[30,31] If the reconstructing point source is at a different distance from the CDOE than any of the two recording point sources were, spherical aberration is present. By the appropriate choice of the CDOE radius the spherical aberration can be eliminated,[32] but—since coma is not eliminated in this case—such CDOEs have limited available field angle.

D. Aplanatic CDOEs for Fourier transform

An ideal Fourier transform lens converts an incoming plane wave of arbitrary slant angle into a diffraction-limited spot at the back focal plane, also called the frequency plane. Each incoming plane wave represents a component in the angular spectrum of an input transparency which is placed in the front focal plane, and hence the back focal plane shows the 2D spectrum of the input transparency. The location of each diffraction-limited spot in the frequency plane should therefore be directly proportional to the spatial frequency component of the input transparency which is responsible for the given tilted plane wave. The spatial frequency of a diffraction grating is proportional to the sine of the tilt angle α of the diffracted plane wave, according to the grating relation $\sin\alpha=\lambda\cdot(1/\Lambda)$, where $(1/\Lambda)$ is the spatial frequency of the grating and λ is the illuminating wavelength. It follows that the location of spots at the frequency plane should be proportional to $\sin\alpha$. This condition is exactly fulfilled for an aplanatic CDOE for principal rays.[34] Therefore, aplanatic CDOEs, which are also free of aberrations that grow linearly with the angle, appear to be naturally suited for Fourier transform applications.

For simple aplanatic CDOEs that are recorded with perfect spherical waves, the residual aberrations such as astigmatism and field curvature still impair the performance. In order to achieve minimum spot sizes over a given input angular range, the radius and the phase function of the CDOE need to be optimized.[35,36] For the latter task the so-called analytic raytracing technique[37] was demonstrated.[35,36] This optimization technique can yield a CDOE with low overall aberrations, provided that there is an entrance pupil in front of the CDOE. However, the experimental implementation of such CDOEs is rather complicated, because additional elements, such as computer-generated holograms, are required to produce the desired aspheric phase function on the curved surface.

VI. EXTENSION TO 2D CONCENTRATION/COLLIMATION WITH 3D CDOE SHAPES

As mentioned in Sec. II, according to the terminology of the literature "1D concentration" is achieved by "2D concentrator shapes" $z(x)$, whereas "2D concentration" is achieved by "3D concentrator shapes" $z(x,y)$. This distinction is illustrated in Fig. 23. Figure 23(a) shows a CDOE that concentrates/collimates light in one dimension (along x). This is the CDOE type that was discussed in the preceeding sections. In the present section CDOEs capable of concentration/collimation in 2D (along x and y) will be discussed, as illustrated in Fig. 23(b). We limit our discussion to systems that are symmetrical about the z axis, so that $z(x,y)=z(r)$, where $r=(x^2+y^2)^{1/2}$.

For sources and targets having an axial symmetry the design technique described in Sec. III and IV can be extended to 3D CDOE shapes and 2D concentration/

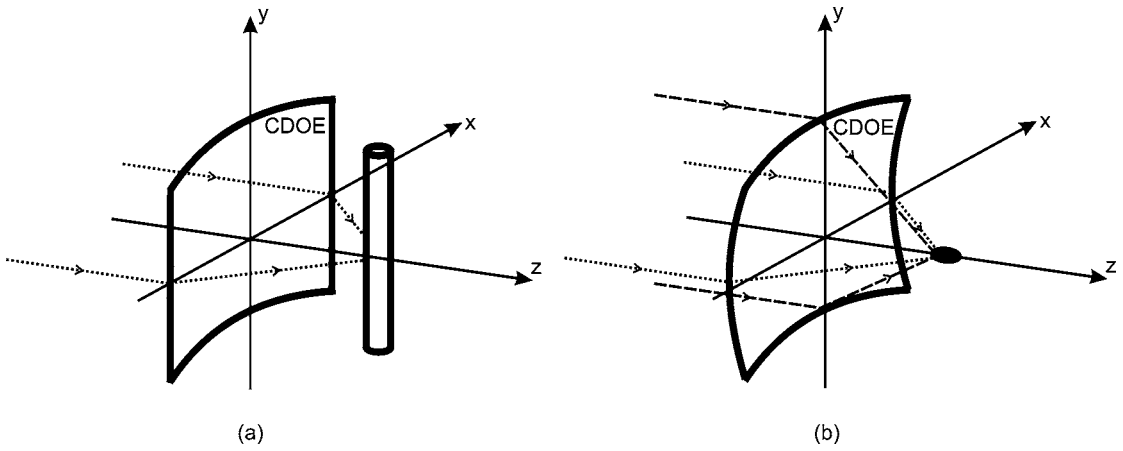

FIG. 23. (a) a CDOE having a "2D shape" (a shape with zero curvature), achieving concentration/collimation in 1D along the x axis, and (b) a CDOE having a cylindrically symmetric "3D shape" (a shape with nonzero curvature), achieving 2D concentration/collimation along x and y. For the 1D concentration/collimation case of (a) the target/source is elongated in the y direction and both the CDOE and the target/source are symmetrical with respect to the (x,z) plane and the (y,z) plane, and for the 2D concentration/collimation case of (b) both the CDOE and the target/source are symmetrical about the z axis.

collimation in a straightforward way.[18] Because of the solid angles involved, the energy conservation Eq. (8) is modified to

$$S(\beta)\cdot\sin\beta\cdot d\beta = I(r)\cdot r\cdot dr, \tag{18}$$

where $S(\beta)$ is defined in the same way as for the 1D case. Similarly, for finite distance concentration the energy conservation Eq. (12) is modified to

$$S_1(\alpha)\cdot\sin\alpha\cdot d\alpha = S_2(\beta)\cdot\sin\beta\cdot d\beta. \tag{19}$$

For Lambertian source and target Eq. (19) can be written as

$$\Delta_1(\alpha)\cdot\sin\alpha\cdot d\alpha = \Delta_2(\beta)\cdot\sin\beta\cdot d\beta, \tag{20}$$

where $\Delta_1(\alpha)$ is the projected area (rather than diameter as in the 1D case) of the source as seen from direction α, and $\Delta_2(\beta)$ is the projected area of the target as seen from direction β.

Solving Eq. (18) for $I(r)$=constant and for a source having a given $S(\beta)$ angular intensity distribution yields a CDOE shape that transforms light coming from the source into a uniform intensity collimated wave, as shown in Fig. 24. For example, for an isotropic point source $[S(\beta)=\text{const.}=F^2]$ the uniform collimator CDOE shape is $r(\beta)=2\cdot F\cdot\sin(\beta/2)$. Interestingly, this CDOE shape is the well-known Herschel surface:[3,4] if the principal surface of a focusing system is a Herschel surface, the system is free of first-order axial aberrations.[1]

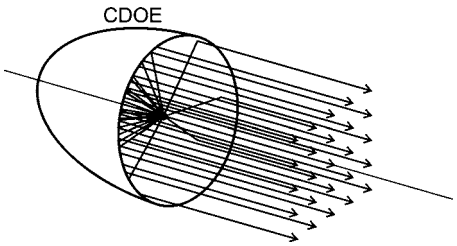

FIG. 24. 3D collimator CDOE shape designed from Eq. (18) with $I(r)$ =constant. The rays are equally spaced in the transverse plane, indicating uniform intensity of the collimated plane wave.

If Eqs. (18)–(20) are used for the design of concentrators onto finite size targets, skew rays—rays that are not in the same plane with the symmetry axis of the system[16]—play an important role in the performance of the concentrator. Skew rays are illustrated in Fig. 25. Each diffuse ray pencil (broken lines) that is in the same plane with the optical axis undergoes diffraction on the local grating (LG) as it is deflected toward the target (T). The diffusive angle of such a ray will change according to the diffraction relation, as described in Secs. III and IV. On the other hand, the diffuse ray pencils hitting the CDOE in the skew direction (dotted lines in Fig. 25) are unaffected by the local grating and are directed toward the target as identical diffuse ray pencils, similarly to simple reflections. Thus, although for infinitesimal source sizes the uniform collimator design Eq. (18) gives correct results, the edge ray principle discussed in the previous sections for elongated Lambertian sources and targets does not apply automatically for 3D CDOE shapes, and hence skew rays may severely impair the concentrating capabilities of the CDOE.

For a flat Lambertian source and a flat Lambertian target the 3D shape design Eq. (20), which takes the form

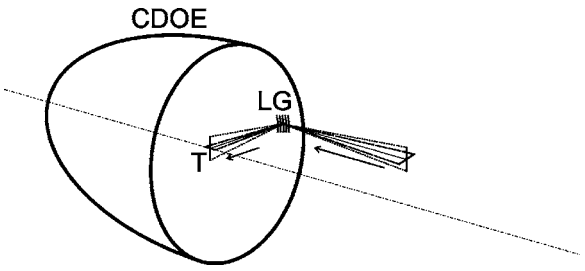

FIG. 25. The effect of skew rays (rays that are not in the same plane with the symmetry axis). The diffuse ray pencils hitting the CDOE in the skew direction (dotted lines) are unaffected by the LG and are directed toward the target (T) as identical diffuse ray pencils, similarly to simple reflections. This is in contrast with diffuse ray pencils that are in the same plane with the symmetry axis (dashed lines). Such ray pencils undergo diffraction on the local grating as they are deflected toward the target, hence their diffusive angle will change according to the diffraction relation, as described in Secs. III and IV.

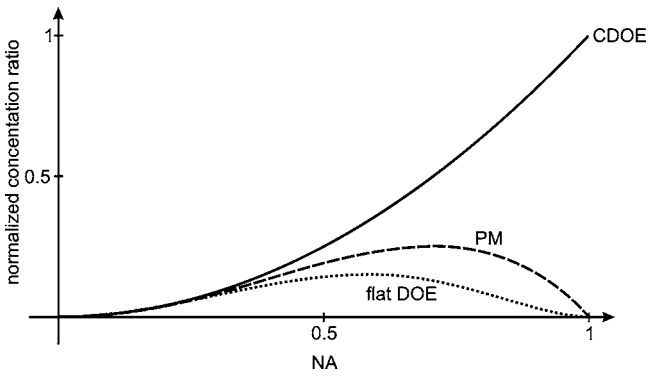

FIG. 26. Calculated normalized concentration ratio for the spherical aplanatic CDOE (solid line), the "3D" flat DOE (dotted line), and the 3D PM (dashed line) as a function of NA (see Fig. 20 for the corresponding graphs of the 2D concentrator shapes). The aplanatic CDOE still reaches the thermodynamic limit at high NA, whereas the maximum achievable concentration ratio for the PM and the flat DOE is 25% (at NA=0.71) and 15% (at NA=0.58) of the thermodynamic limit, respectively.

$$\cos\alpha\cdot\sin\alpha\cdot d\alpha = \mathrm{C}\cdot\cos\beta\cdot\sin\beta\cdot d\beta, \tag{21}$$

leads to the Abbe condition again—here its form is $\sin\alpha/\sin\beta=\sqrt{C}$, where $\sqrt{C}$ is the lateral magnification—just as Eq. (12) did for the 2D CDOE shapes. For this source/target geometry the 3D CDOE shape is spherical and can be thought of as a simple rotated version of the 2D shape.

The Appendix shows that for the spherical aplanatic CDOE skew rays do not pose a problem, because the spot diameters created by skew ray pencils are exactly the same as the perpendicular spot diameters created by the diffracted ray pencils. Thus the spherical aplanatic CDOE is an ideal concentrator onto a flat target in 2D concentration as was shown for the cylindrical aplanatic CDOE in 1D concentration (see Fig. 20, Sec. V). The performance of the aplanatic CDOE in comparison with other concentrators is even more pronounced in the 2D concentration case than in the 1D concentration case, as is illustrated in Fig. 26. Here the three 3D concentrator shapes (corresponding to the three 2D shapes of Fig. 20) are: a spherical CDOE, a 3D PM, and a flat DOE (or, equivalently, a Fresnel zone plate or a refractive lens with a plane principal surface). As shown in Fig. 26, the CDOE satisfying the Abbe condition still concentrates light onto a flat target at the (2D) thermodynamic limit, whereas the maximum concentration ratio achieved by the PM and the flat DOE is 25% and 15% of the thermodynamic limit, respectively.

VII. CONCLUSION

In this article we reviewed the design, optimization and characterization of DOEs fabricated on a curved surface (CDOEs). For such CDOEs not only the phase function, but also the substrate shape are free parameters that can be used for optimization, in many cases yielding much better performances than both flat DOEs and reflective/refractive optical elements when operating with quasimonochromatic light. We showed that CDOEs can be exploited successfully for the specific tasks of collimation/concentration of diffuse light, aberration-free imaging, and optical Fourier transform, where they seem to be ideally suited.

Using the design principle discussed in Secs. III and IV ideal 1D concentration and collimation of diffuse quasimonochromatic light at the thermodynamic limit can be achieved both for infinite (Sec. III) and finite (Sec. IV) distances between the source and the traget. The specific case of flat target/source leads to CDOE shapes satisfying the Abbe condition. For many of the shapes of the source and the target simple analytic expressions exist for the optimal CDOE shape. The design principle can be extended to 2D collimation/concentration having a cylindrical symmetry, but the effect of skew rays must be taken into account, since in some cases (for example for spherical source and target) they severely reduce the concentration efficiency, whereas in other cases (for example for flat source and target) they do not. Finally, the same design principle can be applied for more general beam shaping tasks, for example when a nonuniform intensity distribution of the collimated beam—say a Gaussian one—is desired.

Several experimental realizations were described including 1D diffuse light concentration and aberration-free imaging on a flat target using an aplanatic cylindrical CDOE, and diffuse light concentration on a cylindrical target using a CDOE whose shape is given by Eq. (11). In all these experimental demonstrations the CDOEs were holographically recorded with simple spherical/cylindrical and plane waves and, as expected, the experimental results were much superior to the performance of flat DOEs or parabolic mirrors.

Further numerical optimization of CDOEs using aspherical recording wavefronts is straightforward, but leads to more complicated experimental setups, relying on computer generated holograms,[38] computer-originated holograms[39,40] or recursive recording techniques.[41]

ACKNOWLEDGMENT

The authors would like to thank Ami Ishaaya for his helpful comments.

APPENDIX

1. Proof that the uniform CDOE collimator of Sec. III is also an ideal concentrator

We consider a Lambertian target shown in Fig. 2. The uniform collimator CDOE shape is designed by Eqs. (9) and (10). The CDOE will operate as an ideal concentrator of diffuse light on the Lambertian target, if

$$r(\beta)\cdot\delta(\beta)=\Delta(\beta) \tag{A1}$$

for every β, as seen in Fig. 27. From the conservation of local phase-space area upon diffraction for any DOE:

$$\delta\cdot\sin\left(\frac{3\pi}{2}-\eta-\beta\right)=\epsilon\cdot\sin\left(\eta-\frac{\pi}{2}\right), \tag{A2}$$

which leads to

$$\delta=\epsilon\cdot\frac{1}{\cos\beta-\tan\eta\cdot\sin\beta}. \tag{A3}$$

The slope of the CDOE shape is

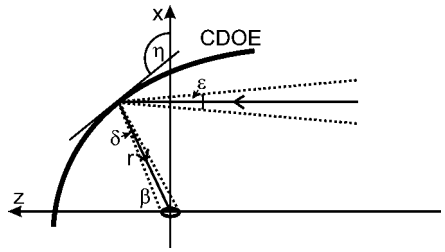

FIG. 27. Uniform collimator CDOE working as a concentrator. The target is placed at the origin. ε is the (full) diffusive angle of the illuminating diffuse beam, δ is the (full) diffusive angle of the diffracted beam directed toward the target located at a distance r from the given CDOE point, and η the angle between the tangent to the CDOE and the x axis.

$$\tan\eta = \frac{dz}{dx} = \frac{dz/d\beta}{dx/d\beta}. \tag{A4}$$

$dx/d\beta$ is now substituted from the design Eq. (9), which for a Lambertian source/target takes the following form:

$$\frac{dx}{d\beta} = C\cdot\Delta(\beta), \tag{A5}$$

where C is a constant; thus $dz/d\beta$ is given by

$$\frac{dz}{d\beta} = \frac{d\left(\frac{x}{\tan\beta}\right)}{d\beta} = \frac{C\cdot\Delta(\beta)}{\tan\beta} - \frac{x}{\sin^2\beta}. \tag{A6}$$

Substituting Eqs. (A5) and (A6) into Eq. (A4) we get

$$\tan\eta = \frac{1}{\tan\beta} - \frac{x}{C\cdot\Delta(\beta)\sin^2\beta}, \tag{A7}$$

and substituting Eq. (A7) into Eq. (A3) we get

$$\delta(\beta) = \epsilon\cdot\frac{C\cdot\Delta(\beta)}{(x/\sin\beta)}, \tag{A8}$$

which yields

$$r(\beta)\cdot\delta(\beta) = \epsilon\cdot C\cdot\Delta(\beta). \tag{A9}$$

Equation (A9) is equivalent to Eq. (A1) with the choice of $C=1/\epsilon$.

2. Proof that the CDOE design Eqs. (13)–(15) yield ideal concentration for finite distances

We only consider the reflection case, shown in Fig. 28. A Lambertian source is placed at A and its diffuse (monochromatic) light is diffracted toward a Lambertian target placed at B, by a CDOE whose shape satisfies Eqs. (13) and (14). For any arbitrary DOE the conservation of local phase-space area upon diffraction yields

$$\delta\cdot\sin\left(\eta+\beta-\frac{\pi}{2}\right) = \epsilon\cdot\sin\left(\frac{3\pi}{2}-\eta-\alpha\right), \tag{A10}$$

which leads to

$$\delta = \epsilon\cdot\frac{\cos(\alpha+\eta)}{\cos(\beta+\eta)} = \epsilon\cdot\frac{\cos\alpha-\sin\alpha\cdot\tan\eta}{\cos\beta-\sin\beta\cdot\tan\eta}. \tag{A11}$$

The slope of the CDOE shape is

$$\tan\eta = \frac{dz/d\alpha}{dx/d\alpha} = \frac{\frac{dr}{d\alpha}\cdot\cos\alpha - r\cdot\sin\alpha}{\frac{dr}{d\alpha}\cdot\sin\alpha + r\cdot\cos\alpha}. \tag{A12}$$

From the design Eqs. (13) and (14) we get

$$\frac{dr}{d\alpha} = d\cdot\frac{\frac{\Delta_1(\alpha)}{\Delta_2(\beta)}\cdot\sin\alpha - \sin\beta\cdot\cos(\alpha-\beta)}{\sin^2(\alpha-\beta)}. \tag{A13}$$

Substituting Eq. (A13) into Eq. (A12) we obtain

$$\tan\eta = \frac{\frac{\Delta_1(\alpha)}{\Delta_2(\beta)}\cdot\sin\alpha\cdot\cos\alpha - \sin\beta\cdot\cos\beta}{\frac{\Delta_1(\alpha)}{\Delta_2(\beta)}\cdot\sin^2\alpha - \sin^2\beta}. \tag{A14}$$

In this case—unlike in Appendix Subsection 1—the diffuse angle ϵ is not constant:

$$\epsilon(\alpha) = \frac{\Delta_1(\alpha)}{r(\alpha)}. \tag{A15}$$

Substituting Eqs. (A14) and (A15) into Eq. (A11) we get

$$\delta(\beta) = \frac{\Delta_2(\beta)\cdot\sin\beta}{r(\alpha)\cdot\sin\alpha} = \frac{\Delta_2(\beta)}{R(\beta)} \tag{A16}$$

for every β, which means that the concentration on the target is ideal.

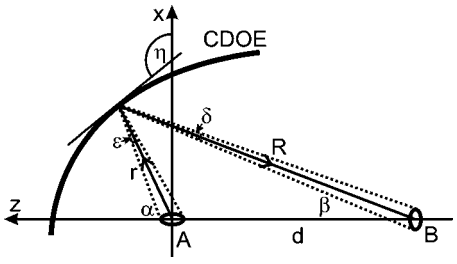

FIG. 28. CDOE working as a concentrator for finite distances. The source (A) and the target (B) are at a distance d from each other. ε is the (full) diffusive angle of the beam emitted by the source, δ is the (full) diffusive angle of the diffracted beam directed toward the target, and η the angle between the tangent to the CDOE and the x axis. R and r are the distances of the target and the source from the given CDOE point, respectively.

3. Proof that for the 3D concentrator CDOE described in Sec. VI skew rays do not impair the performance if the target/source shapes are flat

As discussed in Sec. VI, for flat target and source the design Eq. (20) has the form of Eq. (21), which yields the Abbe condition, i.e., $\sin\alpha/\sin\beta=\text{const}=\sqrt{C}$, where $\sqrt{C}$ is the lateral magnification [C is the "area magnification," as is obvious from Eqs. (20) and (21)]. The CDOE shape is a sphere. Figure 29 shows the circular cross section of such a spherical CDOE—designed for $C=4$—in the (x,z) plane. As seen, diffraction occurs in the (x,z) plane and the skew direction is along the y axis. Since in this specific case the cross sections of the 2D and 3D CDOE shapes are identical, we can use the results of Appendix Subsection 2 to get

$$\frac{X_{\text{out}}}{X_{\text{in}}} = \text{const} = \sqrt{C}, \tag{A17}$$

independently of α, where X_{in} and X_{out} are the source and target diameters along x. Relation (A17) is the combined

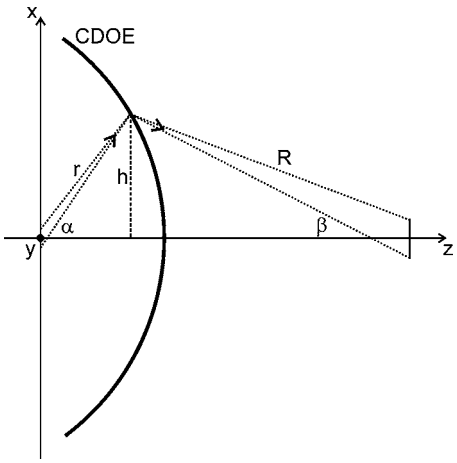

FIG. 29. Circle-shaped cross section of a spherical aplanatic CDOE working as a concentrator for finite distance. Both the source and the target are flat. Diffraction occurs in the (x,z) plane and the skew direction is along the y axis. Since the spot sizes are identical in the diffractive and in the skew directions, the performance of such a spherical aplanatic CDOE is not affected by skew rays.

result of diffraction and the slanted projection of target and source in the ray directions.

In the skew direction, i.e., along y, none of these effects are present, and the ray pencil simply undergoes reflection upon the CDOE. Because of the sine condition

$$\frac{R}{r} = \frac{h/r}{h/R} = \frac{\sin\alpha}{\sin\beta} = \sqrt{C}. \tag{A18}$$

For a given point on the CDOE the diffusive angle of the input skew ray pencil is $\epsilon_{\text{skew}} = Y_{\text{in}}/r$, where Y_{in} is the source diameter along y. The spot diameter on the target along y is $Y_{\text{out}} = R \cdot \epsilon_{\text{skew}}$, yielding

$$\frac{Y_{\text{out}}}{Y_{\text{in}}} = \frac{R}{r} = \text{const} = \sqrt{C}, \tag{A19}$$

independently of α. As seen from Eqs. (A17) and (A19), the spherical CDOE operates in the same way in the diffractive and in the skew directions.

[1] M. Born and E. Wolf, *Principles of Optics* (Pergamon, Oxford, 1993).
[2] R. Kingslake, *Lens Design Fundamentals* (Academic, New York, 1978).
[3] N. Bokor and N. Davidson, Opt. Lett. **29**, 1968 (2004).
[4] C. J. R. Sheppard and P. Török, J. Mod. Opt. **44**, 803 (1997).
[5] I. M. Bassett, W. T. Welford, and R. Winston, in *Progress in Optics*, edited by E. Wolf (North-Holland, Amsterdam, 1989), Vol. 27, pp. 161–226.
[6] N. Bokor and N. Davidson, J. Opt. Soc. Am. A **19**, 2479 (2002).
[7] N. Bokor and N. Davidson, in *Progress in Optics*, edited by E. Wolf (North-Holland, Amsterdam, 2005).
[8] H. A. Rowland, Am. J. Sci. **26**, 87 (1883).
[9] W. T. Welford, in *Progress in Optics*, edited by E. Wolf (North-Holland, Amsterdam, 1965), Vol. 4, pp. 241–280.
[10] G. Schmahl and D. Rudolph, in *Progress in Optics*, edited by E. Wolf (North-Holland, Amsterdam, 1976), Vol. 14, pp. 197–244.
[11] D. G. McCauley, C. E. Simpson, and W. J. Murbach, Appl. Opt. **12**, 232 (1973).
[12] N. Davidson and N. Bokor, Opt. Lett. **29**, 1318 (2004).
[13] N. Davidson, A. A. Friesem, E. Hasman, and I. Shariv, Opt. Lett. **16**, 1430 (1991).
[14] N. Bokor and N. Davidson, Appl. Opt. **40**, 5825 (2001).
[15] Y. Xie, Z. Lu, F. Li, J. Zhao, and Z. Weng, Opt. Express **10**, 1043 (2002).
[16] R. Winston and W. T. Welford, *High Collection Nonimaging Optics* (Academic, New York, 1989).
[17] N. Davidson and N. Bokor, in *Progress in Optics*, edited by E. Wolf (North-Holland, Amsterdam, 2003), Vol. 45, pp. 1–51.
[18] N. Davidson and N. Bokor, J. Opt. Soc. Am. A **21**, 656 (2004).
[19] W. T. Welford, Opt. Commun. **9**, 268 (1973).
[20] N. Bokor, R. Shechter, A. A. Friesem, and N. Davidson, Opt. Commun. **191**, 141 (2001).
[21] E. M. Kritchman, A. A. Friesem, and G. Yekutieli, Appl. Opt. **18**, 2688 (1979).
[22] E. M. Kritchman, A. A. Friesem, and G. Yekutieli, Sol. Energy **22**, 119 (1979).
[23] M. V. R. Murty, J. Opt. Soc. Am. **50**, 923 (1960).
[24] W. T. Welford, Opt. Commun. **15**, 46 (1975).
[25] K. Tatsuno, Opt. Rev. **4**, 203 (1997).
[26] E. Jagoszewski, Optik (Jena) **69**, 85 (1985).
[27] E. Jagoszewski and M. Klakoćar-Ciepacz, Optik (Jena) **72**, 165 (1986).
[28] K. O. Peng and H. J. Frankena, Appl. Opt. **25**, 1319 (1986).
[29] P. E. Verboven and P. E. Lagasse, Appl. Opt. **25**, 4150 (1986).
[30] J. Nowak and M. Zajac, Opt. Appl. **18**, 51 (1988).
[31] E. Jagoszewski and A. Talatinian, Optik (Jena) **88**, 155 (1991).
[32] S. Baskar and K. Singh, J. Mod. Opt. **39**, 1533 (1992).
[33] A. L. Belostotsky and A. S. Leonov, J. Lightwave Technol. **11**, 1314 (1993).
[34] E. Jagoszewski and A. Talatinian, Optik (Jena) **88**, 20 (1991).
[35] A. Talatinian, Opt. Appl. **21**, 19 (1991).
[36] A. Talatinian, Optik (Jena) **89**, 151 (1992).
[37] E. Hasman and A. A. Friesem, J. Opt. Soc. Am. A **6**, 62 (1989).
[38] W. H. Lee, in *Progress in Optics*, edited by E. Wolf (North-Holland Amsterdam, 1978), Vol. 16, pp. 119–232.
[39] R. C. Fairchild and R. J. Fienup, Opt. Eng. (Bellingham) **21**, 133 (1982).
[40] S. Reinhorn, Y. Amitai, and A. A. Friesem, Appl. Opt. **37**, 3031 (1998).
[41] Y. Amitai and A. A. Friesem, J. Opt. Soc. Am. A **5**, 702 (1988).